

LIQUEFACTION HAZARD MAPPING USING GEOSTATISTICAL METHOD IN RICHMOND, BRITISH COLUMBIA, CANADA

A. Javanbakht⁽¹⁾, S. Molnar⁽²⁾, A. Sadrekarimi⁽³⁾

⁽¹⁾ Graduate Student, Department of Earth Sciences, University of Western Ontario, ajavanba@uwo.ca

⁽²⁾ Assistant Professor, Department of Earth Sciences, University of Western Ontario, smolnar8@uwo.ca

⁽³⁾ Associate Professor, Department of Civil and Environmental Engineering, University of Western Ontario, asadrek@uwo.ca

Abstract

Southwestern British Columbia is one of the most seismically active regions in Canada and due to soil conditions, particularly silty sands and high level of water table in some regions of Greater Vancouver, soil liquefaction could be one of the most destructive consequences from future strong earthquake shaking. Liquefaction hazard maps are increasingly being incorporated into earthquake risk mitigation practice and used for urban planning and site selection of engineering structures. Liquefaction potential index (LPI) is an appropriate choice for spatial analysis of liquefaction hazards as it shows good correlation with surface manifestations of liquefaction. Over 180 cone penetration test (CPT) soundings are compiled to calculate the safety factor against liquefaction using a deterministic M 7.5 shallow earthquake scenario. LPI values are obtained and categorized into five liquefaction hazard classifications. Spatial interpolation of LPI across the northwestern Fraser River delta region is accomplished using a kriging method based on an empirical exponential semivariogram model from the CPT-based LPI calculated values. The resulting deterministic liquefaction hazard map is presented for our M 7.5 shallow earthquake scenario. For most areas, liquefaction potential shows high and very high hazard. Box and whisker plots are used to compare LPI distributions and their statistics for four geology units of the study area. The geologic units show broad LPI distributions that have significant overlap between units. The Fraser River delta unit which contains mostly sands and silty sands corresponds to the highest LPI values as expected. The probability of liquefaction-induced ground disruption is also evaluated. When the occurrence probability is greater than 0.5, the probability of liquefaction-induced ground disruption is higher than that without induced liquefaction. For most of the investigated northwestern Fraser River delta, a probability of liquefaction-induced ground disruption is predicted.

Keywords: liquefaction hazard mapping; CPT; liquefaction potential index; kriging; probability of liquefaction

1. Introduction

Simplified methods for predicting seismic triggering of liquefaction [1] determine whether a soil layer at a specific depth liquefies, but it does not provide the severity of liquefaction. Factor of safety (FS) against liquefaction for each soil layer in the simplified procedure is defined as the ratio of cyclic resistance ratio (CRR) to cyclic stress ratio (CSR). Ishihara [2] stated that the soil liquefaction potential at a specific site is dependent on the thickness of liquefied and non-liquefied layers. If a non-liquefied layer is thinner than the underlying liquefied layer, then liquefaction will occur for this soil profile. A better liquefaction prediction metric, inclusive of liquefaction severity, is liquefaction potential index (LPI) proposed by Iwasaki et al. [3] which determines the liquefaction potential along a soil profile from ground surface to a depth of 20 m. Soil liquefaction potential decreases with depth as effective stress increases with depth. LPI is an appropriate choice for spatial analysis of liquefaction hazards as it enables two-dimensional mapping of a three-dimensional measure and has been shown to correlate well with surface manifestations of liquefaction [4]. The surface effects from liquefaction at depths greater than 20 m are rarely reported.

Iwasaki et al. [3] stated that the thickness of the liquefied layer, proximity of the liquefied layer to ground surface, and amount by which the FS is less than 1 are contributing factors to define liquefaction severity. They evaluated LPI at 85 sites in Japan for six liquefaction-triggering earthquakes based on standard penetration testing (SPT) blow counts measured at 1 m interval spacing and determined that severe liquefaction occurred when LPI is greater than 15 and no liquefaction occurred for sites with $LPI < 5$. Thus, LPI values range from 0 for a site with no liquefaction potential to 100 for a site with factor of safety less than 1 along the entire 20-m soil profile. Liquefaction severity was categorized by Iwasaki et al. [3] into four hazard rankings of very low ($LPI = 0$), low ($0 < LPI \leq 5$), high ($5 < LPI \leq 15$) and very high ($LPI > 15$). In addition, non-liquefiable regions could not be distinguished using this classification and a moderate hazard category is lacking. To solve these issues, Sonmez [5] added a moderate liquefaction hazard category by modifying the threshold FS value between non-liquefiable and marginally-liquefied categories from 1.0 to 1.2; soil layers with $FS > 1.2$ and between 1.0 and 1.2 are considered as non-liquefied and marginally-liquefiable soils, respectively [6, 7]. Seed and Idriss [8] suggested that values of 1.25 to 1.5 for safety factor against liquefaction are acceptable for non-liquefiable soils.

Liquefaction hazard maps increasingly are being incorporated into earthquake risk mitigation practice and are used for planning stages of urban settlement areas and site selection of engineering structures. Early regional liquefaction hazard mapping relied on surficial geology of the region, current mapping relies on geotechnical investigations such as cone penetration testing (CPT) and SPT along with surficial geology. Regional liquefaction hazard mapping is commonly accomplished using LPI in many regions [4, 9, 10, 11, 12]. Toprak and Holzer [4] examined field observations of empirical liquefaction of the 1989 Loma Prieta earthquake in comparison to LPI calculated using 50 CPTs at 20 sites. The LPI values > 5 were correlated with the occurrence of sand boils and LPI values > 12 were correlated with lateral spreading occurrences. $LPI > 5$ is generally accepted as a threshold value for surface damage of liquefaction by Iwasaki et al. [3], Topark and Holzer [4] and Holzer et al. [13]. Luna and Frost [14] used the LPI metric to generate a liquefaction potential map for Treasure Island, a hydraulic fill island in San Francisco Bay, California, and compared the values to surface liquefaction damage from the 1989 Loma Prieta earthquake. Holzer et al. [13] presented a liquefaction hazard map based on cumulative frequency distributions of LPI per surficial geologic unit based on CPT and SPT measurements along the eastern shore of San Francisco Bay, including the city of Oakland. Lenz and Baise [15] investigated CPT- and SPT-based liquefaction potential considering LPI criteria across the East San Francisco Bay and demonstrated the use of kriging as a geostatistical method to interpolate between data points to generate liquefaction hazard maps.

The regional geology of Metro Vancouver consists of Tertiary and older bedrock with variable Quaternary sediments consisting of Pleistocene glaciated tills and Holocene sediments. The municipality of Richmond, south of Vancouver, is mainly situated on deposits of the Fraser River delta which has been building out into the Strait of Georgia since the end of the last glaciation [16]. Liquefaction features have been observed at numerous sand dykes during foundation excavation at the Kwantlen College campus in Richmond, British Columbia. These sand dykes were caused by one or more large earthquake induced liquefaction and originated in a shallow fine to medium grained sand [17].

In this study, over 180 CPT profiles in Richmond city of Metro Vancouver, British Columbia, Canada are used to obtain factor of safety against liquefaction for each layer along the 20 m maximum CPT profile based on the latest simplified methodology of Boulanger and Idriss [1]. We calculate LPI for a shallow North American crustal scenario earthquake with magnitude 7.5 in the Strait of Georgia, northwest and offshore of Vancouver. A geostatistical spatial interpolation (kriging) of CPT-based LPI values across the region is accomplished to generate a preliminary liquefaction triggering potential map of Richmond as a part of the Metro Vancouver seismic hazard mapping project [18, 19]. The Institute for Catastrophic Loss Reduction (ICLR) and the University of Western Ontario with support from Emergency Management British Columbia (EMBC) are working together to generate comprehensive earthquake hazard maps for the Metro Vancouver region of British Columbia [18, 19].

2- Methodology

Southwestern British Columbia is a tectonically active region in Canada with nearby populated urban environments such as Metropolitan (Metro) Vancouver. This region is located over the subducting Juan de Fuca plate at the northern extent of the Cascadia subduction zone and is subject to frequent earthquakes. In this study, a deterministic approach towards liquefaction hazard mapping is performed selecting a single earthquake magnitude and focus (epicentre location). We select a shallow crustal earthquake scenario with magnitude 7.5 in the Strait of Georgia at a depth of 10 km, 50 km northwest and offshore of Vancouver; this is a common large magnitude scenario for the region [20]. For each soil layer of the 183 CPT profiles across Richmond, CSR for our selected scenario earthquake event is calculated based on the simplified method proposed by Seed and Idriss [21] from Eq. (1):

$$CSR = \frac{\tau_{av}}{\sigma'_{v0}} = 0.65 \left(\frac{a_{max}}{g} \right) \left(\frac{\sigma_{v0}}{\sigma'_{v0}} \right) r_d \quad (1)$$

where a_{max} is the peak ground acceleration, g is the acceleration of gravity, r_d is the stress reduction factor proposed by Idriss [22] in extending the work of Golesorkhi [23], σ_{v0} and σ'_{v0} are total and effective vertical stresses respectively at the depth of interest, and τ_{av} is average cyclic shear stress. Peak ground acceleration (PGA) is derived from ground motion models for site class C and then site factors provided in 2015 NBCC (National Building Code of Canada) are applied to convert to site class E. To calculate total and effective vertical stresses, soil unit weights are estimated from a correlation by Robertson and Cabal [24].

The municipality of Richmond is mainly situated on deposits of the Fraser River delta as shown in Fig 1a. Salish Sea and Fraser River sediments are the two distinct Holocene sediments that are well distributed in Richmond. Salish sediments consists of marine shore, lacustrine, alluvial and deltaic deposits of smaller rivers which were formed in post-glacial time. Fraser River sediments consists of marine and fluvial sediments that are deposited from 9000 ka to recent. Fraser River sediments consists of bottomset deposits of thick silt and clay up to 120 m, foreset deposits of sandy silt up to 165 m thick, and topset deposits of thick sand between 8-30 m thickness. The maximum thickness of Holocene deposits in Richmond is 300 m. Holocene Fraser River (F) and Salish (S_A) sediments are subdivided further into seven geologic units (Fig. 1b) based on depositional environment [25]. The unit S_{Aa} is comprised of landfills having sand, gravel, till, crushed stone, swamp and shallow lake deposits. S_{Ab} is about 14 m thick lowland peat. S_{Ac} is lowland peat up to 1 m thick. S_{Ad} unit is composed of 0.15 to 0.45 m thick lowland organic sandy loam to clay loam. F_a unit is channel deposits which varies from fine to medium sand with minor silt occurring along river channels. F_b unit is overbank sandy to silty clay loam up to 2 m thick which overlay about 15 m of deltaic and distributary channel fill (F_d). F_c is overbank silty to silt clay loam up to 2 m thick present in eastern Richmond.

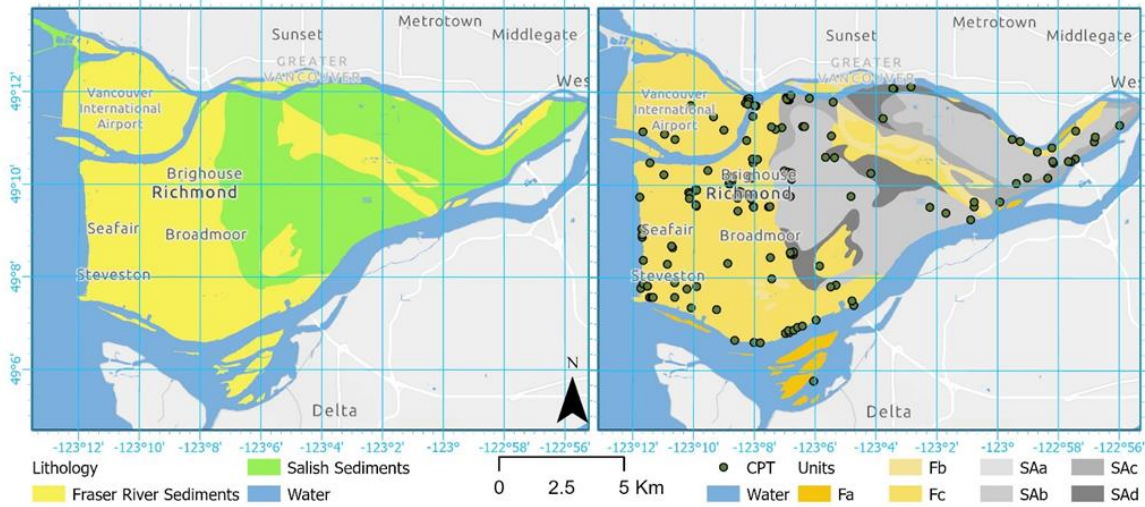


Fig. 1 – (a) Simplified Quaternary geology map of Richmond and (b) locations of CPT data (circles) shown with the detailed Quaternary geology map of Richmond.

A total of 183 CPT profiles are present in the Richmond area from our compiled regional geodatabase [26]. Fig. 1b shows the location of these CPTs with the Quaternary surficial geological units of Richmond. Of these 183 CPT soundings, 127 are in F_c, 19 in S_{Ab}, 18 in S_{Ac}, 15 in S_{Ad}, 3 in F_b and 1 in S_{Aa}. The advantage of using CPT data is its ability to measure a relatively continuous soil profile (centimeter scale) as well as locating thin layers of potentially liquefiable soils that can be missed by SPT. CRR is the resistance provided by the soil, dependent on soil type and density determined from geotechnical (*in situ* and laboratory) testing. To determine CRR, we extract CPT tip resistance (q_c) and sleeve friction (f_s) values up to 20 m depth from the 183 CPT soundings at 5 cm depth intervals. Of the 183 CPT soundings, 153 (83%) reach the 20 m depth. Of the soundings that do not reach 20 m, 20 CPT profiles terminate at 15-20 m and 10 CPTs reach depths of 10-15 m. The CPT profiles with depths of less than 10 m are not considered in our study because they may bias our LPI values towards lower values (5 CPTs were removed). Depth of the ground water table for each CPT site is taken from *in situ* measurements if reported, or extracted from a regionally interpolated map of ground water table depth for Metro Vancouver [26]. Unsaturated soil above the ground water table is not evaluated here using the simplified procedure.

The measured cone tip resistance is corrected for pore water pressure acting on the cone (u_2) to obtain the corrected total cone resistance, q_c . For sandy soils, the magnitude of this correction is small, while in soft clay layers is significantly large. In our analyses, pore water correction is applied whenever the value of u_2 is measured and we use the term q_c with understanding that the correction has been performed [1]. For defining soil type of each layer from CPT measurements, the soil behavior type index (I_c) proposed by Robertson and Cabal [24] is used. I_c is calculated via normalized cone resistance and sleeve friction ratios considering the stress exponent n which changes from 0.5 in sands to 1.0 in clays. The stress exponent n in determining I_c varies with soil type and stress level and it is computed from relationship by Robertson [27] and this new formula captures the correct *in situ* state at high stress level. In this study, if I_c is greater than 2.60, then the soil has too much fines content (too clayey) to liquefy. We note that Youd et al. [28] suggests that soil layers with $I_c > 2.4$ should be sampled and tested to investigate the soil behavior type. The CPT procedure requires normalization of tip resistance called dimensionless cone penetration resistance q_{c1N} . CPTs are corrected for overburden stress effects with Eq. (2):

$$q_{c1N} = C_N q_{cN} = C_N \frac{q_c}{P_a} \quad (2)$$

where C_N is overburden correction factor and P_a (=101.325 kPa) is atmospheric pressure. The C_N calculation by Boulanger [29] is dependent on equivalent clean sand penetration resistance (q_{c1Ncs}) and requires an iterative procedure which we accomplish in an Excel spreadsheet using Eqs. (3a and 3b):

$$C_N = \left(\frac{P_a}{\sigma'_v}\right)^m \leq 1.7 \quad (3a)$$

$$m = 1.338 - 0.249(q_{c1Ncs})^{0.264} \quad (3b)$$

The normalized tip resistance for silty sands should be corrected to an equivalent clean sand value (q_{c1Ncs}) applying correction factor for grain characteristics. The equivalent clean sand adjustment, Δq_{c1N} is considered in this simplified method for the effect of fines content (FC) on cyclic stress ratio and cone penetration resistance from Boulanger and Idriss [1]. Δq_{c1N} and q_{c1Ncs} are estimated from Eqs. (4 and 5):

$$\Delta q_{c1N} = \left(11.9 + \frac{q_{c1N}}{14.6}\right) \exp\left(1.63 - \frac{9.7}{FC+2} - \left(\frac{15.7}{FC+2}\right)^2\right) \quad (4)$$

$$q_{c1Ncs} = q_{c1N} + \Delta q_{c1N} \quad (5)$$

Experiences show that defining FC from correlation with I_c is problematic. Therefore, it is suggested that every CPT sounding should be accompanied by one borehole with soil samples to perform laboratory tests for defining FC. We obtained FC from adjacent boreholes and if FC data are not provided in geotechnical reports, then the relationship by Boulanger and Idriss [1] is used to estimate FC from Eq. (6):

$$FC = 80(I_c + C_{FC}) - 137 \quad (6)$$

$$0\% \leq FC \leq 100\%$$

where C_{FC} is a fitting parameter to estimate FC. The revised relationship for magnitude scaling factor (MSF) by Boulanger and Idriss [1] is used in evaluating liquefaction triggering potential; our $M_w = 7.5$ earthquake scenario corresponds to a MSF of 1. The overburden correction factor, K_σ , developed by Boulanger [29] is applied in FS calculation with Eq. (7):

$$K_\sigma = 1 - C_\sigma \ln\left(\frac{\sigma'_v}{P_a}\right) \leq 1.1 \quad (7)$$

$$C_\sigma = \frac{1}{37.3 - 8.27(q_{c1Ncs})} \leq 0.3$$

CRR is calculated from deterministic version of CPT-based relationship by Boulanger and Idriss [1] in Eq. (8) and safety factor against liquefaction is computed from Eq. (9) for each 5 cm depth interval along the CPT profile. The value of 1.2 is selected as the threshold FS value between marginally liquefied condition and non-liquefiable categories [5].

$$CRR_{M=7.5, \sigma'_v=1atm} = \exp\left(\frac{q_{c1Ncs}}{113} + \left(\frac{q_{c1Ncs}}{1000}\right)^2 - \left(\frac{q_{c1Ncs}}{140}\right)^3 + \left(\frac{q_{c1Ncs}}{137}\right)^4 - 2.80\right) \quad (8)$$

$$FS = \left(\frac{CRR_{7.5}}{CSR}\right) K_\sigma MSF \quad (9)$$

LPI obtained from Eq. (10) represents the cumulative liquefaction potential of the soil column from ground surface to 20 m depth, where z is the depth from ground surface in meters and $w(z) = 10 - 0.5z$ is a depth weighting factor linearly decreasing from 10 at surface to 0 at a depth of 20 m, and F_L is liquefaction factor which depends on safety factor against liquefaction:

$$LPI = \int_0^{20} F_L w(z) dz \quad (10)$$

$$\begin{aligned} F_L &= 0 & FS &\geq 1.2, \\ F_L &= 1 - FS & FS &\geq 0.95, \\ F_L &= 2 \times 10^6 e^{-18.427FS} & 1.2 &> FS > 0.95 \end{aligned}$$

The discretized form of LPI calculation for continuous CPT profiles by Luna and Frost [30] is used in Eq. (11); where H_i is each 0.05 m CPT depth interval and n is the number of soil layers:

$$LPI = \sum_{i=1}^n w_i F_{Li} H_i \quad (11)$$

Fig. 2 shows an example of CPT data and LPI calculation for one site. For this CPT sounding, ground water table is at 2.5 m depth and the uppermost layer with 4 m thickness is mostly clay and silty clay with FC too high against liquefaction. Thick liquefiable sandy layers and silty sands at greater than 5.5 m depth cause a significant increase in LPI value reaching to above 25.

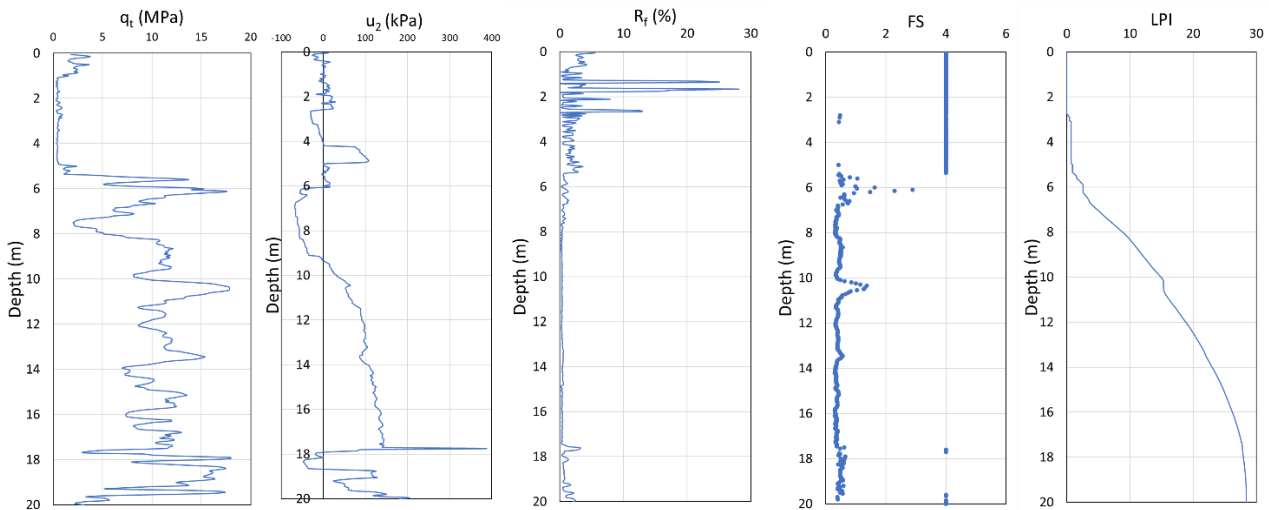


Fig. 2 – An example for one CPT site in Richmond showing (left to right) total cone resistance, pore water pressure behind cone, friction ratio, factor of safety against liquefaction and LPI with depth.

In this study, liquefaction hazard rating is assigned based on calculated LPI according to Table 1 which shows the liquefaction hazard classification of Iwasaki et al. [3] including the two additional categories, moderate and non-liquefiable, proposed by Sonmez [5].

Table 1- Liquefaction hazard classification scheme proposed by Sonmez [5].

Liquefaction Potential Index (LPI)	Liquefaction hazard category
0	Non-liquefiable
$0 < LPI \leq 2$	Low
$2 < LPI \leq 5$	Moderate
$5 < LPI \leq 15$	High
$LPI > 15$	Very High

LPI values are grouped by surficial geology to determine LPI distributions within each surficial geology unit. Box and whisker plots are used to show LPI distributions for each surficial geology unit to compare their five-number statistical summary: minimum, maximum, median, the first (Q_1) and the third quartile (Q_3) values. Holzer et al. [13] proposed that surface manifestation of liquefaction occurs when LPI is > 5 and we use this criterion to evaluate the approximate percentage of liquefied area for each geologic unit applying cumulative frequency graph. The main assumption of this methodology is that each geologic unit is considered statistically homogenous. For generating the liquefaction hazard map, the first step is applying direct interpolation of LPI values with geostatistical analysis in ArcGIS Pro using an empirical exponential semivariogram model with nugget variance shown in Eq. (12):

$$\text{Semivariogram (distance } h) = \frac{1}{2} \times \text{average}[(LPI_{\text{location}_i} - LPI_{\text{location}_j})^2] \quad (12)$$

This semivariogram model determines the spatial correlation distance of our calculated LPIs which is used to estimate LPIs via kriging interpolation throughout Richmond. In this way, we generate our preliminary liquefaction triggering potential hazard map of Richmond based on LPI.

3. Liquefaction hazard

3.1 LPI values and LPI distribution within geology units

The simplified method (equations 1 to 9) is used to obtain safety factor against liquefaction and then LPI is calculated (equation 11) for 183 CPT sites within the Richmond area. Our LPI calculations determine 92% of our CPT sites in the Richmond area have LPI > 5 (high and very high liquefaction-triggering potential hazard), 79% have LPI > 15 (very high hazard), 4.4% have LPI between 2 and 5 (moderate hazard), and 4.9% of sites show LPI < 2 (low hazard).

Variability in LPI within four Holocene geologic units (F_c , S_{Ab} , S_{Ac} , S_{Ad}) and all Holocene units combined is evaluated using box and whisker plots in Fig. 3. F_c and S_{Ab} have the highest values of LPI, while S_{Ad} and S_{Ac} correspond to lower values of LPI. There are 127 CPT profiles in the F_c unit. Box and whisker plots are not generated for the smaller LPI populated Holocene units F_a , F_b and S_{Aa} . S_{Ab} has the largest span of LPI values with a Q_1 of 7.5 and Q_3 of 42.5. In addition, a significant overlap between the three Salish sediment geologic units is observed. The Fraser River geology unit corresponds to the highest LPI values. Detailed exploration of this geologic unit's soil profiles reveals that high LPI values (>15) result from liquefiable silty sands and layers of liquefiable sands within thin layers of non-liquefied clay. A ground water table near ground surface at most Fraser River sediment sites also increases the liquefaction-triggering potential hazard. The Q_1 and Q_3 LPI values of this F_c unit are 27 and 41, respectively.

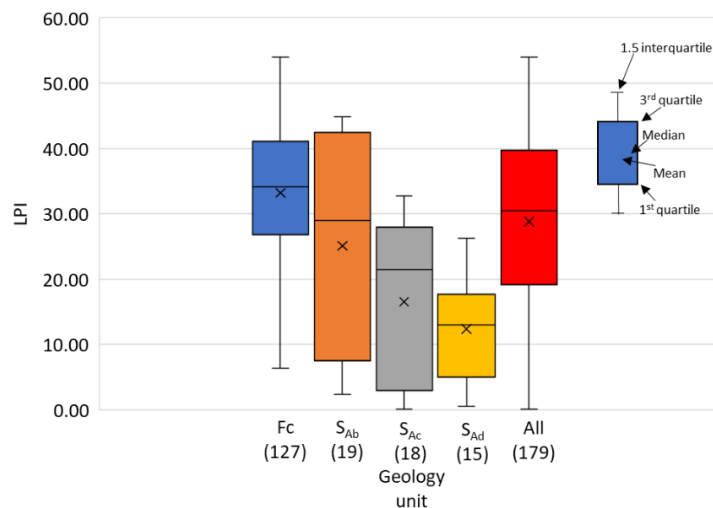


Fig. 3 – LPI distribution for four Holocene geologic units and all Holocene units combined. Numbers in parentheses report the number of CPT profiles.

Table 2 lists the median and mean LPI values for each Holocene geologic unit. F_c and S_{Ab} units have higher mean and median values of LPI, while mean and median values for S_{Ad} are the lowest. Mean values for F_c and S_{Ab} are 33 and 25, respectively. It is worth noting that in terms of liquefaction hazard rating, three units (F_c , S_{Ab} and S_{Ac}) are rated very high and one unit (S_{Ad}) as high considering mean and median values.

Table 2- LPI statistics for each applicable Holocene geologic unit.

Geologic Unit	Mean LPI	Median LPI
F _c	33	34
S _{Ab}	25	29
S _{Ac}	16	18
S _{Ad}	11	12

The percentage of surface area within each geologic unit exhibiting surface damage of liquefaction ($LPI \geq 5$) is estimated using cumulative frequency distributions. Fig. 4 presents the cumulative LPI frequency for the four applicable Holocene geologic units and all Holocene units combined. For the M 7.5 earthquake scenario, 56% of the areas within the S_{Ac} unit will show surface manifestations of liquefaction. This increases to 73% and 79% of areas in S_{Ad} and S_{Ab} units respectively, and 100% of the areas in the F_c unit. Instead of defining the percentage area exhibiting surface manifestation of liquefaction, the cumulative frequency of $LPI \geq 5$ can be interpreted as the conditional probability of liquefaction at a specific location [13]. For instance, the prediction of liquefaction in 56% of the areas underlain by unit S_{Ac} can be interpreted as a 56% probability that a randomly selected location underlain by S_{Ac} unit will show surface effects of liquefaction.

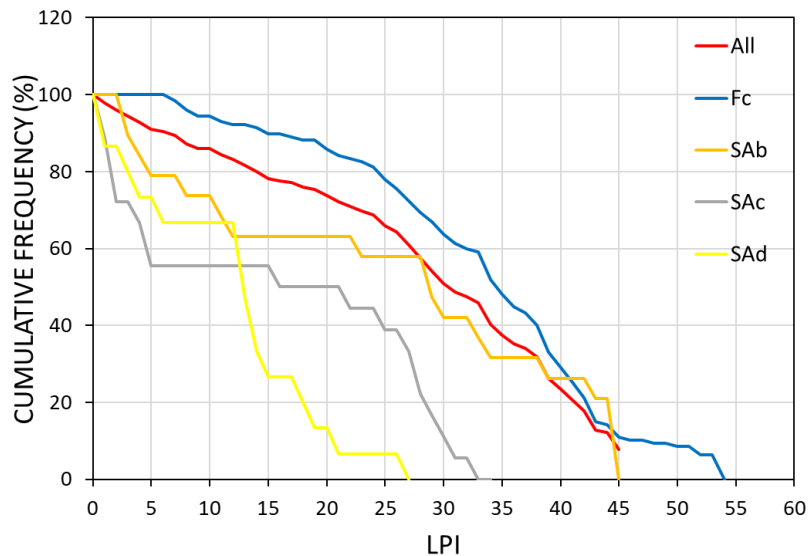


Fig. 4- Cumulative frequency distribution of LPI for four Holocene geologic units and all Holocene units combined.

3.2 Liquefaction hazard mapping with LPI

The LPI values calculated across the study area are shown in Fig. 5 in comparison to the Holocene geologic units and coloured according to the liquefaction hazard categorization of Table 1. Most of the LPI values are > 15 and classified into the very high hazard group. In south central Richmond, some sites have slightly lower LPI values between 5 and 15 representing high hazard classification. Locations of low and moderate hazard ratings are present in eastern Richmond related to the presence of thick peat deposits. Spatial gaps are present and additional CPT soundings in these areas would be beneficial.

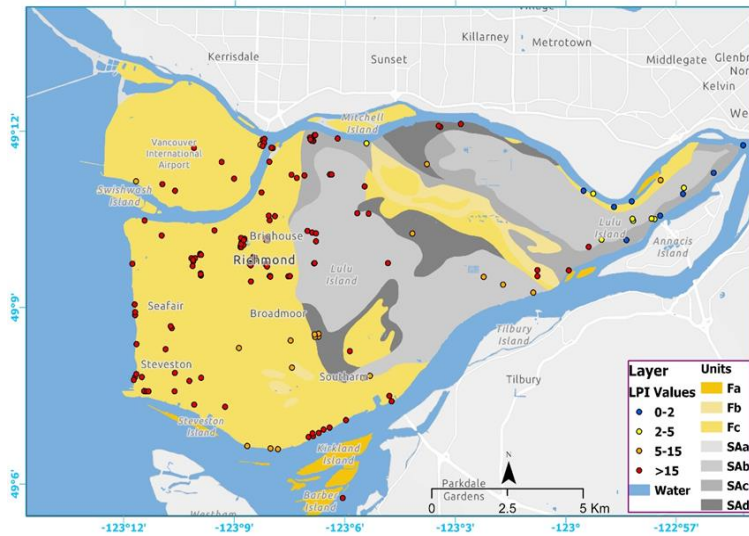


Fig. 5 – Map showing liquefaction hazard rating based on LPI across Richmond.

Empirical Bayesian kriging is applied to estimate interpolated values of LPI from neighbourhood points and produce a spatially interpolated liquefaction hazard map. An exponential semivariogram model is used, which is typical for soil parameters which are expected to have a low variance [15]. A preliminary liquefaction-triggering potential hazard map of Richmond based on LPI given a M 7.5 shallow crustal earthquake in the Strait of Georgia is shown Fig. 6. Western and central Richmond is dominated by very high liquefaction hazard with shallow ground water table, while some areas in central and southern Richmond correspond to high liquefaction hazard. The young sand layers in southern Richmond relate to high and very high hazard of liquefaction. Another factor that generates high and very high hazard is thick layers of interbedded sands and silts. An area in northern Richmond, trending southeast of Mitchell Island (east of the Airport Island), is classified as high hazard. In eastern Richmond, peat layers varying from 1 to 10 m thick result in moderate and low liquefaction hazard. The peat layers are not liquefiable and show very low cone resistance. Overall Fraser River sediments correspond to very high and high liquefaction hazard for our M 7.5 shallow earthquake scenario. Salish sediments have variable liquefaction hazard, ranging from low hazard in eastern Richmond to high hazard in northeast Richmond. In most areas, our liquefaction hazard rating is generally similar to the categorization used in the liquefaction hazard map of Richmond by Monahan [31], however, different criteria were used to generate their map.

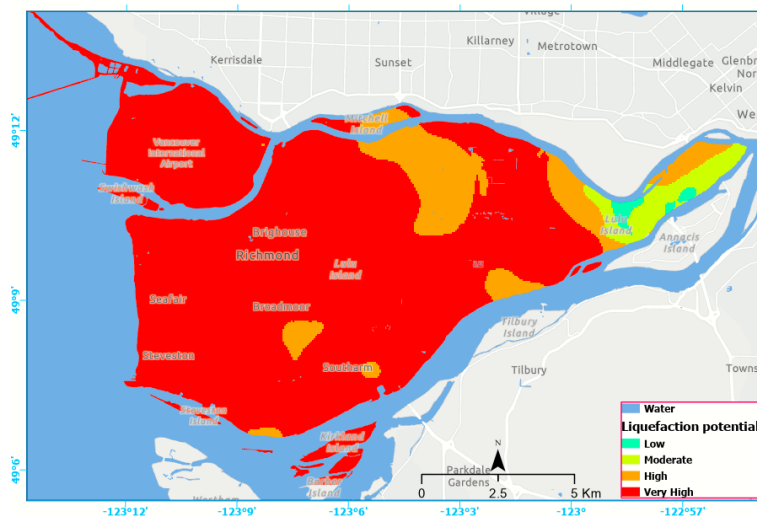


Fig. 6 – Preliminary liquefaction hazard map based on LPI for Richmond considering a M 7.5 shallow earthquake scenario.

3.3 Probability of liquefaction occurrence

The LPI values for each CPT sounding are used in the relationship proposed by Papathanassiou [32] to estimate the probability of liquefaction-induced surface disruption with Eq. (13):

$$Prob (liquefaction) = \left(\frac{1}{1 + e^{-(-3.092 + 0.218 \times LPI)}} \right) \quad (13)$$

The occurrence probabilities of a dichotomy event are between 0 for non-occurrence of liquefaction and 1 for the occurrence of liquefaction. When the occurrence probability is greater than 0.5, the probability of liquefaction occurrence is higher than that of without liquefaction. In other words, at sites with $Prob (liq) \geq 0.5$ liquefaction-induced surface disruption is predicted to occur, while sites with $Prob (liq) < 0.5$ non-occurrence of liquefaction is expected [33]. All deterministic LPI values calculated for Richmond are applied in Eq. (13); the value of LPI corresponding to the boundary $Prob (liq) = 0.5$ is equal to 14.2 [32]. Sites with $LPI > 14.2$ correspond to a higher probability of liquefaction-induced surface disruption than the probability of non-liquefaction. Fig. 7 shows the probability of liquefaction-induced surface disruption based on LPI values across Richmond.

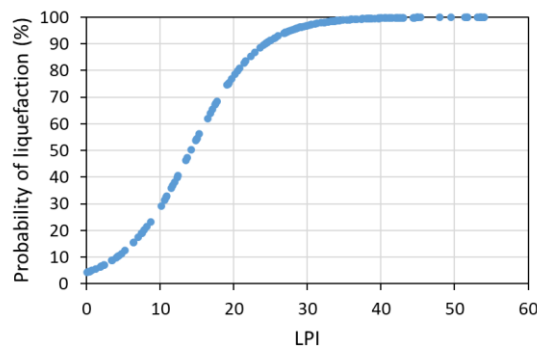


Fig. 7- Probability curve of deterministic LPI values in Richmond.

Fig. 8 shows the spatial distribution of the calculated probability of liquefaction-induced ground disruption given our selected M 7.5 earthquake scenario. The occurrence probability of liquefaction in almost all areas of western and southern Richmond is greater than 0.5. Therefore, the probability of liquefaction-induced surface disruption is higher in these areas. The probability of liquefaction-induced surface disruption in eastern Richmond city is low.

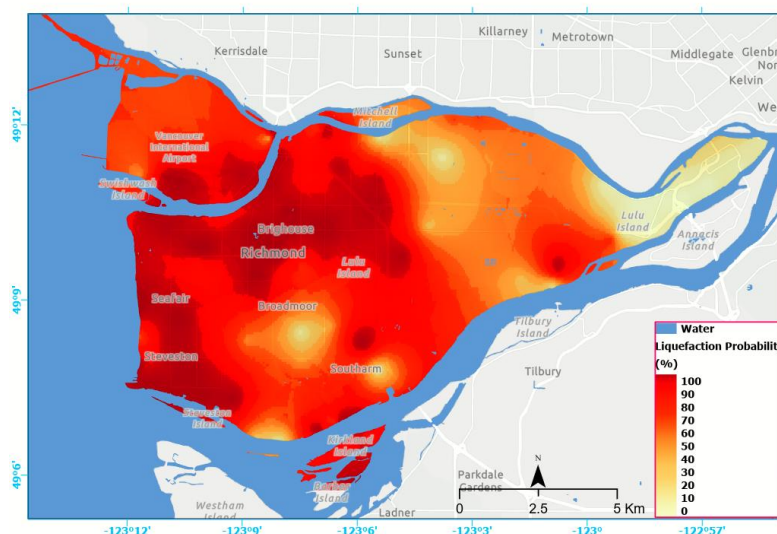


Fig. 8- The probability map of liquefaction-induced ground disruption considering a M 7.5 shallow earthquake scenario.

4. Conclusion

Over 180 CPT profiles are used to determine LPI values across Richmond, British Columbia, Canada for a deterministic M 7.5 shallow earthquake scenario. Most (92%) of the LPI-calculated sites correspond to high and very high liquefaction-triggering potential hazard. The percentage of areas predicted to be liquefied within S_{Ac} unit is the lowest at 56%, while all areas underlain by the Fraser River F_c geologic unit will exhibit surface manifestations of liquefaction. Upper sandy and silty sand layers of the Fraser River delta are liquefiable and contribute significantly to increase LPI values. In eastern Richmond, moderate and low hazards of liquefaction-triggering potential are predicted based on the presence of peat deposits. For our given earthquake scenario, the probability of liquefaction-induced disruption in most areas of Richmond is higher than the non-occurrence of liquefaction probability. This paper documents our preliminary efforts in calculating and using LPI in the generation of liquefaction hazard maps for the Metro Vancouver seismic hazard mapping project. A deterministic earthquake scenario, dependent on the selected magnitude and its peak ground acceleration, was performed in this study. A probabilistic approach which considers all earthquake magnitude contributions to the peak ground acceleration, consistent with 2015 and 2020 Canadian seismic design guidelines, is under investigation.

Acknowledgements

We thank Sujan Adhikari for his help to improve the quality of maps and we gratefully acknowledge multiple agencies, organizations, municipalities, and individuals that provided both public and private sources of CPT data to the Metro Vancouver seismic microzonation project. Funding provided by the Institute for Catastrophic Loss Reduction (ICLR) with support from Emergency Management British Columbia (EMBC).

References

- [1] Boulanger RW, Idriss IM (2016): CPT-Based Liquefaction Triggering Procedure. *J. Geotech. Geoenviron. Eng.*, **142** (2), 11
- [2] Ishihara, K (1985): Stability of natural deposits during earthquakes. *In: Proceedings of the 11th International Conference on Soil Mechanics and Foundation Engineering*, San Francisco, CA, USA, **1**, 321–376.
- [3] Iwasaki T, Tokida K, Tatsuoka F, Watanabe S, Yasuda S, Sato H (1982): Microzonation for soil liquefaction potential using simplified methods. *In: Proceedings of the third international earthquake microzonation conference, vol. III*. Seattle, WA, 1319–30.
- [4] Toprak S, Holzer TL (2003): Liquefaction potential index: field assessment. *J Geotech Geoenviron Eng.*, **129** (4), 315–22.
- [5] Sonmez H (2003): Modification of the liquefaction potential index and liquefaction susceptibility mapping for a liquefaction-prone area (Inegol, Turkey). *Environ Geol*, **44** (7), 862–71.
- [6] Tosun H, Ulusay R (1997): Engineering geological characterization and evaluation of liquefaction susceptibility of foundation soils at a dam site, southwest Turkey. *Environ Eng Geosci*, **3** (3), 389–409.
- [7] Ulusay R, Kuru T (2004): 1998 Adana–Ceyhan (Turkey) earthquake and a preliminary microzonation based on liquefaction potential for Ceyhan town. *Natural Hazards*, **32**, 59–88.
- [8] Seed HB, Idriss IM (1982): *Ground motions and soil liquefaction during earthquakes*. Earthquake Engineering Research Institute, University of California, Berkeley.
- [9] Papathanassiou G, Pavlides S, Ganas A (2005): The 2003 Lefkada earthquake: field observation and preliminary microzonation map based on liquefaction potential index for the town of Lefkada. *Engineering Geology*, **82**, 12–31.
- [10] Heidari T, Andrus RD (2010): Mapping liquefaction potential of aged soil deposits in Mount Pleasant. *South Carolina Engineering Geology*, **112** (1), 1-12.
- [11] Kang GC, Chung JW, Rogers JD (2014): Re-calibrating the thresholds for the classification of liquefaction potential index based on the 2004 Niigata-ken Chuetsu earthquake. *Engineering Geology*, 2014; **169**, 30-40.

- [12] Rahman MZ, Siddiqua S, Kamal ASMM (2015): Liquefaction hazard mapping by liquefaction potential index for Dhaka City, Bangladesh. *Eng Geol*, **188**, 137–147.
- [13] Holzer, T L, Bennett MJ, Noce TE, Padovani AC, Tinsley JC (2006): Liquefaction hazard mapping with LPI in the greater Oakland, California, area. *Earthquake Spectra*, **22** (3), 693–708.
- [14] Luna R, Frost JD (2000): Treasure Island’s spatial liquefaction evaluation. *Geotech Spec Publ* 2000 (93), 306–20.
- [15] Lenz JA, Baise LG, (2007): Spatial variability of liquefaction potential in regional mapping using CPT and SPT data. *Soil Dynamics and Earthquake Engineering*. **27**, 690–702.
- [16] Clague JJ, Lutemauer JL, Mosher, DC (1998): Geology and natural hazards of the Fraser River Delta, British Columbia. *Geological Survey of Canada*, 525, 270.
- [17] Naesgaard, E, Sy, A., and Clague, J.J. 1992. Liquefaction sand dykes at Kwantlen College, Richmond, B.C. *In Geotechnique and natural hazards*, BiTech Publishers, Vancouver, B.C., 159.166.
- [18] Metro Vancouver seismic microzonation project, <https://www.metrovanmicromap.ca>
- [19] Molnar S, Assaf J, Sirohey A, Adhikari SR (2020): Overview of local site effects and seismic microzonation mapping in Metropolitan Vancouver, British Columbia, Canada. *Engineering Geology, Special Issue on Seismic site response estimation for microzonation studies promoting the resilience of urban centers*, Volume **270** (5), 105568.
- [20] Journeay JM, Dercole F, Mason D, et al. (2015): A profile of earthquake risk for the district of North Vancouver, British Columbia. *Geological Survey of Canada Open File 7677*, Ottawa, ON, Canada, Natural Resources Canada.
- [21] Seed HB, Idriss IM, (1971): Simplified procedure for evaluation soil liquefaction potential. *Journal of the Soil Mechanics and Foundations Division*, ASCE 97, 1249–1273 SM9.
- [22] Idriss IM (1999): An update to the Seed-Idriss simplified procedure for evaluating liquefaction potential. *In Proceedings, TRB Workshop on New Approaches to Liquefaction*, Publication No. FHWARD-99-165, Federal Highway Administration, January.
- [23] Golesorkhi R (1989): Factors influencing the computational determination of earthquake-induced shear stresses in sandy soils, Ph.D. thesis, University of California at Berkeley, 395 pp.
- [24] Robertson PK, Cabal KL (2015): *Guide to cone penetration testing for geotechnical engineering*. Gregg drilling. 6th edition.
- [25] Armstrong JE (1984): Environmental and engineering applications of the surficial geology of the Fraser Lowland, British Columbia. *Geological Survey of Canada*, **54**, 83-23.
- [26] Adhikari SR, Molnar SE, Wong J (2021): Significance of geodatabase development for seismic microzonation in Metropolitan Vancouver, Canada. *17th World Conference on Earthquake Engineering, Sendai*, Japan Paper No: 4521.
- [27] Robertson PK (2009a): Interpretation of cone penetration tests – a unified approach. *Canadian Geotechnical Journal*, **46**, 1337-1355.
- [28] Youd TL, Idriss IM, Andrus RD, Arango I, Castro G, Christian JT, et al. (2001): Liquefaction resistance of soils: summary report from the 1996 NCEER and 1998 NCEER/NSF workshops on evaluation of liquefaction resistance of soils. *J Geotech Geoenviron Eng*, **127** (10), 817–33.
- [29] Boulanger RW (2003b): High overburden stress effects in liquefaction analyses, *J. Geotechnical and Geoenvironmental Eng.*, ASCE **129** (12), 1071–082.
- [30] Luna R, Frost JD (1998): Spatial liquefaction analysis system. *J Comput CivEng*, **12** (1), 48–56.
- [31] Monahan AP, Levson VM, Kerr B (2010): *Liquefaction hazard map of Richmond, British Columbia*. Geoscience Map 2010-3.
- [32] Papathanassiou G (2008): LPI-based approach for calibrating the severity of liquefaction-induced failures and for assessing the probability of liquefaction surface evidence, *Engineering Geology*, **96**, 94-104.
- [33] Bourenane H, Bouhadad Y, Tas M (2017): Liquefaction hazard mapping in the city of Boumerdès, Northern Algeria. *Bull Eng Geol Environ*, 1–17.